Computers in Biology and Medicine 113 (2019) 103420

Contents lists available at ScienceDirect

Computers in Biology and Medicine

journal homepage: http://www.elsevier.com/locate/compbiomed

Automated segmentation of villi in histopathology images of placenta

S. Salsabili [a,*], A. Mukherjee [b,c], E. Ukwatta [a,d], A.D.C. Chan [a], S. Bainbridge [e,f], D. Grynspan [g]

[a] Department of Systems and Computer Engineering, Carleton University, Ottawa, Ontario, Canada
[b] Interdisciplinary School of Health Sciences, University of Ottawa, Ottawa, Ontario, Canada
[c] Department of Pathology and Laboratory Medicine, Children's Hospital of Eastern Ontario, Ottawa, Ontario, Canada
[d] School of Engineering, University of Guelph, Guelph, Ontario, Canada
[e] Department of Cellular and Molecular Medicine, University of Ottawa, Ontario, Canada
[f] Interdisciplinary School of Health Sciences, University of Ottawa, Ontario, Canada
[g] Department of Pathology and Laboratory Medicine, Children's Hospital of Eastern Ontario and the University of Ottawa, Ontario, Canada

ARTICLE INFO

Keywords:
Histopathology
Biomedical image processing
Placenta
Image segmentation
Preeclampsia
Color image processing

ABSTRACT

Purpose: Manual analysis of clinical placenta pathology samples under the microscope is a costly and time-consuming task. Computer-aided diagnosis might offer a means to obtain fast and reliable results and also substantially reduce inter- and intra-rater variability. Here, we present a fully automated segmentation method that is capable of distinguishing the complex histological features of the human placenta (*i.e.*, the chorionic villous structures).

Methods: The proposed pipeline consists of multiple steps to segment individual placental villi structures in hematoxylin and eosin (H&E) stained placental images. Artifacts and undesired objects in the histological field of view are detected and excluded from further analysis. One of the challenges in our new algorithm is the detection and segmentation of touching villi in our dataset. The proposed algorithm uses the top-hat transformation to detect candidate concavities in each structure, which might represent two distinct villous structures in close proximity. The detected concavities are classified by extracting multiple features from each candidate concavity. Our proposed pipeline is evaluated against manual segmentations, confirmed by an expert pathologist, on 12 scans from three healthy control patients and nine patients diagnosed with preeclampsia, containing nearly 5000 individual villi. The results of our method are compared to a previously published method for villi segmentation.

Results: Our algorithm detected placental villous structures with an F1 score of 80.76% and sensitivity of 82.18%. These values are substantially better than the previously published method, whose F1 score and sensitivity are 65.30% and 55.12%, respectively.

Conclusion: Our method is capable of distinguishing the complex histological features of the human placenta (*i.e.*, the chorionic villous structures), removing artifacts over a large histopathology sample of human placenta, and (importantly) account for touching adjacent villi structures. Compared to existing methods, our developed method yielded high accuracy in detecting villi in placental images.

1. Introduction

The human placenta is a vital organ of pregnancy, exchanging all gases, nutrients, and waste products between the mother and developing fetus. This complex organ is essential for fetal survival. Developmental abnormalities and/or in utero damage to this organ can have detrimental short- and long-term health effects for both the mother and her fetus. Placental damage or dysfunction is known to play a central role in the development of fetal intrauterine growth restriction, pre-term birth, stillbirth, preeclampsia, and has also been linked to long term health outcomes, such as premature cardiovascular disease in mothers and metabolic disturbances in offspring [1–8]. The effective application of placental histopathology following a poor pregnancy outcome can inform ongoing clinical management of mothers and neonates, and offer insight into etiology of placental disease, the risk of recurrence in future pregnancies, and may provide indications regarding which mothers and offspring are at highest risk of cardio-metabolic disease later in life [9–14]. However, unlike some other fields of clinical pathology, there are a limited number of perinatal pathologists who are highly specialized in the field of placental histopathology, and the quality and

* Corresponding author.
E-mail address: sina.salsabili@carleton.ca (S. Salsabili).

https://doi.org/10.1016/j.compbiomed.2019.103420
Received 22 May 2019; Received in revised form 12 August 2019; Accepted 27 August 2019
Available online 30 August 2019

reproducibility of placental pathology examinations are currently very poor [15–17]. Collectively, this has limited the clinical utility of this diagnostic/prognostic tool. The ability to apply an unbiased quantitative approach to the field of placental histopathology would substantially reduce the high degree of inter-observer variability and quality control issues currently plaguing this field [18–20], allowing for highly reproducible and reliable findings from this clinical modality. It is anticipated that the contextually rich information that could be gained from automated forms of placental histopathology would allow for a highly integrated use of placenta pathology findings in the continuum of care – allowing for effective translation of findings from the microscope to the clinical management of mothers and babies.

In recent years, there has been increased interest in and research addressing automated detection and analysis of various features within the complex architecture of the human placenta [21–26]. The chorionic villi are the basic functional units of the placenta, anatomically described as a branched "tree-like structure" covered in a multinucleated layer of syncytiotrophoblast cells, which encases the feto-placental vasculature, embedded within a non-cellular connective tissue core. These villi structures are bathed in maternal blood, found within the intervillous space, in vivo. Previous work has focused on automated detection of the feto-placental vascular space within the villi – as poor feto-placental vascular development has been linked to several obstetrical diseases. Almoussa et al. [22] used a segmentation approach based on artificial neural networks (ANNs) to automatically extract feto-placental blood vessel features from digital histological images of the placenta. The ANNs were successful in detecting these most prominent vascular spaces within the placental villi. Chang et al. [25] proposed an automatic filtering method, which locally detects pixels containing curvilinear structures and reduces non-vessel noise. Compared to ANN-based methods, Chang et al. [25] proposed a faster and more accurate approach for feto-placental vessel detection.

A fuzzy C-means clustering method was applied successfully to distinguish cellular vs. extracellular components of the chorionic villi and to identify areas normally filled with maternal blood (intervillous space) [26]. Kidron et al. [24] used ImageJ software (https://imagej.net/) to extract features, such as size and number of chorionic villi, from histological images of the placenta and tested the feasibility of automated diagnosis of delayed or accelerated villous maturation. However, the images analyzed appear to be selective (*e.g.*, there was no indication that artifacts in the histological images were present). In addition, this method does not appear to properly segment villi that are in very close proximity, touching, or overlapping (*e.g.*, Fig. 1 in Kidron et al. [24] shows touching villi identified as a single villous structure). Swiderska-Chadaj et al. [23] described a method of automatic segmentation of placental villi structures for assessment of edema within the placenta. These authors used texture analysis, mathematical morphology, and region growing operations to extract different structures from placental images. Although they presented a comprehensive pipeline for automated analysis of placental histology, a small sample size of 50 villi from placentas with a variety of pathologies was used, with selective/optimal image selection (e.g., no image artifacts).

The objective of this paper is to describe an image analysis pipeline for automated analysis and segmentation of chorionic villi structures in histopathology images of human placentas. The main contribution of this work is the development of a new automated, segmentation protocol, which operates with a high degree of accuracy over large sample size. We also address the issue of adjacent, touching, and overlapping chorionic villi in our work, a common clinical finding that has not been properly addressed in the literature. The proposed method is validated on a set of healthy control placentas, as well as those complicated with the placenta-mediated disease of preeclampsia, to ensure the developed algorithm performs effectively for analyzing placenta specimens from healthy and diseased subjects. We also compare our work with a previously published automated method to detect villi in histological images of the placenta [24]. We apply their provided source code to our dataset and compare the results to our method.

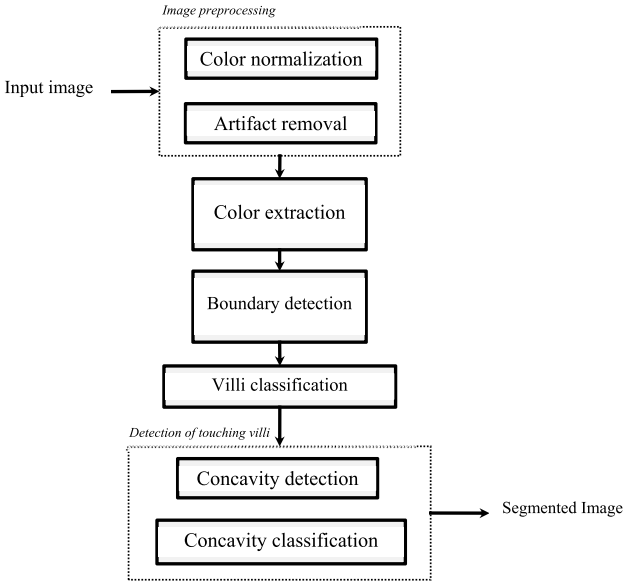

Fig. 1. Block diagram of our methodology.

2. Methodology

2.1. Placenta histopathology images

Our dataset comprises high-resolution digital scans of 12 placental histopathology specimens obtained from the Research Centre for Women's and Infants Health (RCWIH) Biobank (Mount Sinai Hospital, Toronto, ON). The ethics approval to perform sub-analyses on the Biobank samples was obtained from the Ottawa Health Science Network Research Ethics Board and the Children's Hospital of Eastern Ontario (CHEO) Research Ethics Board.

The placental specimens were fixed in paraffin wax, stained with hematoxylin, washed in a 0.3% acid alcohol solution, and counterstained with eosin following the standard protocol for hematoxylin and eosin (H&E) staining at the Department of Pathology and Laboratory Medicine at the CHEO. Slides were scanned (Aperio Scan Scope), and high-resolution color images ($20\times$ magnification) were obtained. In total, 12 placental scans were generated from three healthy term placental specimens and nine placental specimens collected from term pregnancies complicated with preeclampsia (PE). From each placental scan, three sample images of size 2740×3964 pixels were extracted, amounting to a total of 36 sample images (nine images from healthy term pregnancies and 27 from term pregnancies complicated with PE).

Manual segmentation of these images was performed using ImageJ software by A.M. and verified by D.G. (a clinical perinatal pathologist). For each sample image, a "chorionic villi mask" was manually generated by A.M (verified by D.G), identifying individual villi structures and artifact objects. These masks were generated by manually drawing a line around the area of each target object (*i.e.*, villi or undesired objects). The manual segmentation provided an estimation of adjacent villi boundaries and boundaries of undesired objects (*i.e.*, objects that are not considered villi). The manual segmentation served as a ground truth for training and evaluation. From the 36 sample images, there were 4946 villi in total.

2.2. Image segmentation

The image processing pipeline for villi segmentation in a placental image is shown in Fig. 1. The various steps are discussed in detail below.

2.3. Image preprocessing

A number of factors can contribute to variations in the color content of histological images (e.g., histochemical staining time, amount of histology stain used, etc.). We applied a comprehensive color normalization [27] to input images to compensate for such variations. Imaging artifacts might also exist in the histological images. In our work, imaging artifacts appeared as darkened areas of the image, and therefore needed to be removed prior to segmentation of the villi boundary. In Fig. 4 a, examples of these imaging artifacts are identified with blue arrows. Using Equation (1), pixels that are part of the imaging artifacts were identified; the intensity of these pixels was then adjusted to be white.

$$\begin{cases} bw_1(k,l) = \left|I_i(k,l) - I_j(k,l)\right| \le C1 \\ bw_2(k,l) = \left|I_i(k,l)\right| \le C2 \\ BW_{artifact} = bw_1 \cap bw_2 \\ where \begin{cases} i \ne j \\ i,j \in (R,G,B) \\ k \in (1,m), l \in (1,n) \end{cases} \end{cases} \quad (1)$$

In equation (1), I is an $m \times n \times 3$ intensity matrix and $I_i = \begin{bmatrix} a_{1,1} & \cdots & a_{1,n} \\ \vdots & \ddots & \vdots \\ a_{m,1} & \cdots & a_{m,n} \end{bmatrix}$ represents the ith matrix in RGB color space (i.e., red, green, and blue). The constant c_1 is a threshold to ensure that the intensity differences between the R, G, and B channels are small (*i.e.*, detected pixel is essentially grey). The constant c_2 is a threshold to ensure the detected pixels are relatively dark. The values assigned to c_1 and c_2 were 5 and 200, respectively, which were determined empirically. The $BW_{artifact}$ is a binary mask, which is the intersection of the bw_1 and bw_2 binary masks and contains all of the pixels in I that are contaminated with artifacts, which are adjusted to be white.

2.4. Color extraction

Pixels in the histological images of the placenta were divided into three classes based on color: red, white, and purple. Examples of these color classes and their subdivisions can be seen in Fig. 2. The first step in color classification is the extraction of the white class, found primarily outside of the villi, which is the maternal side of the placenta, called the intervillous space. This is deemed the background of the image. White spaces also exist within the core of some villi, primarily made of a non-cellular compartment of mesenchymal connective tissue (MCT) and/or tears in the connective tissue, which represent no specific tissue compartment. The white class is extracted using equation (2):

$$\begin{cases} bw_1(k,l) = \left|I_i(k,l) - I_j(k,l)\right| \le C3 \\ bw_2(k,l) = \left|I_i\right| \ge TH \\ BW_{white} = bw_1 \cap bw_2 \\ where \begin{cases} i \ne j \\ i,j \in (R,G,B) \\ k \in (1,m),\ l \in (1,n) \end{cases} \end{cases} \quad (2)$$

In equation (2), TH is a threshold, whose value is determined using Otsu's method [28]. This threshold ensures that the extracted pixels have high intensities (close to white). The constant $C3$ is a threshold to ensure that the intensity difference between the R, G, and B channels is small. The value assigned to $C3$ was 15, which was determined empirically. The BW_{white} is a binary mask, which is generated by the intersection of bw_1 and bw_2 binary masks, and contains the white class pixels.

The second step was the extraction of the red class. The red regions represent areas rich in fetal red blood cells, found within the feto-placental blood vessels encased within villi. In this work, all placental samples were washed several times during histological processing to remove blood from the tissue; however, some red blood cells often remain in each specimen. The combination of the red and white regions within the core of villi is referred to as the villi core (VC). The realization of the red class transformation is illustrated in Fig. 3. A transformed matrix T is computed (equation (3)), which highlights the red class, and a threshold is applied to extract the red class. The value for this threshold "TH" is determined using Otsu's method [28].

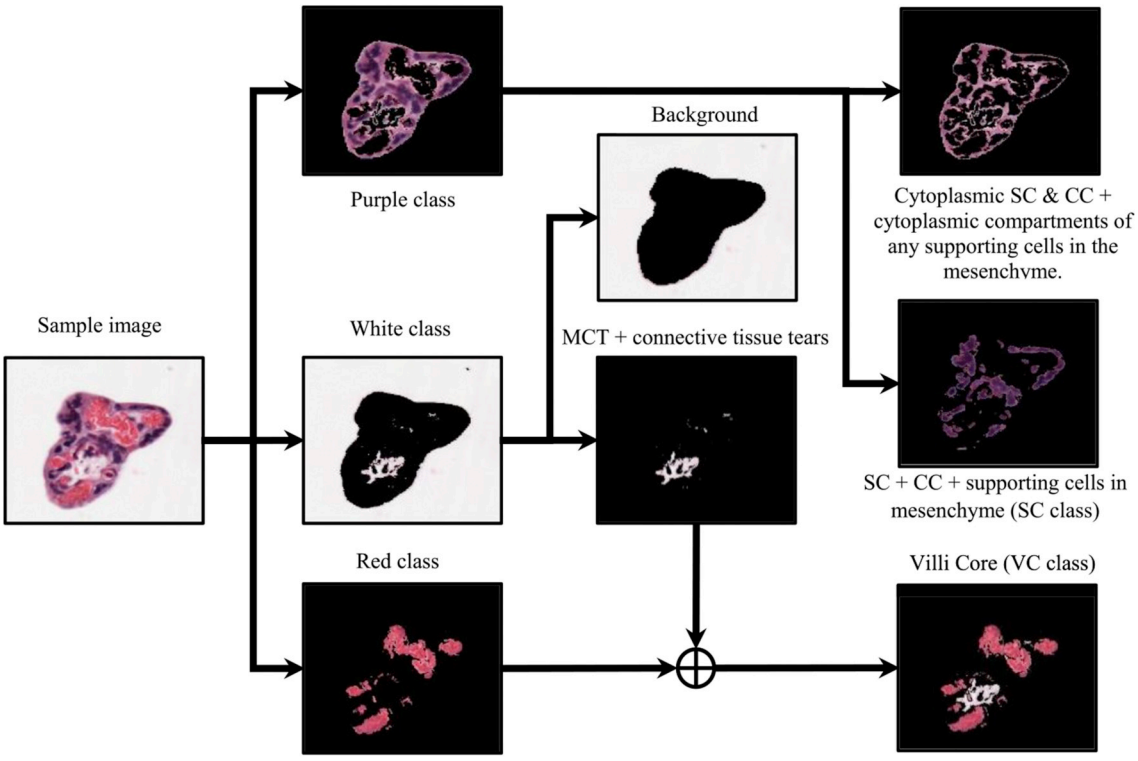

Fig. 2. Classification of color content in H&E stained images, including: syncytiotrophoblasts cells (SC) and cytotrophoblasts cells (CC) in the purple class; non-cellular mesenchymal connective tissue (MCT) in the white class; and fetal red blood cells within the villi core vasculature in the red class.

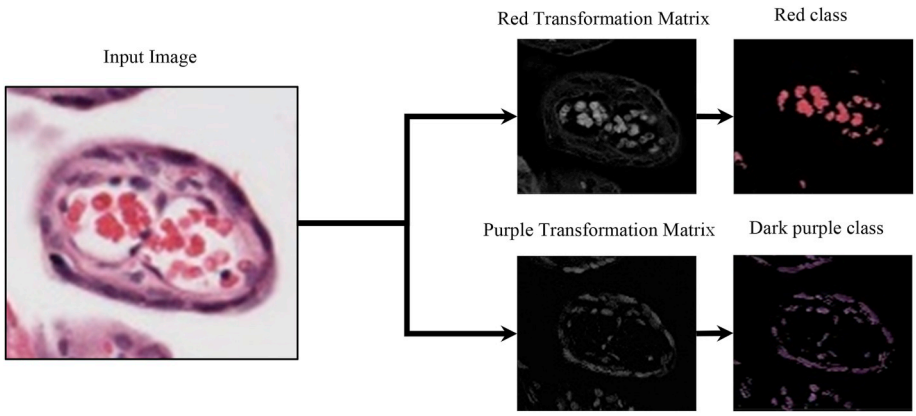

Fig. 3. Example of the red and dark purple class color extraction.

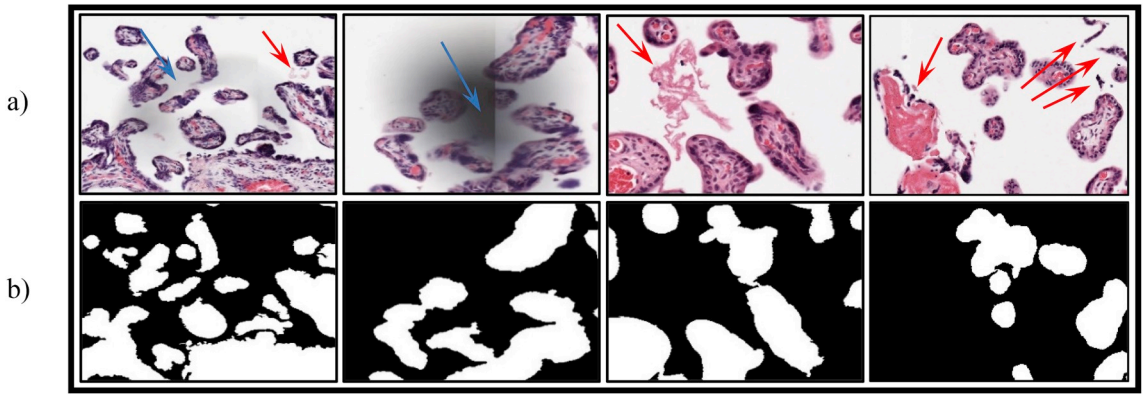

Fig. 4. a) Examples of artifacts and undesired objects. The blue arrows show the areas that are affected by artifacts and the red arrows show the undesired objects. b) the villi classification steps output that shows the removal of artifacts and undesired objects.

$$\begin{cases} T \triangleq I_R - mean(I_G + I_B) \\ BW_{red} = (T \geq TH) \end{cases} \quad (3)$$

The remaining pixels are assigned to the purple class, which represents several other cellular compartments. The dark purple regions primarily identify the nuclei of the syncytiotrophoblasts cells (SC), cytotrophoblasts cells (CC), along with the nuclei of any supporting cells, which might be present in the mesenchyme connective tissue core (i.e., fibroblasts, immune cells). SCs and CCs are densely packed along the villi borders. Nuclei of mesenchymal support cells, on the other hand, have a sparse appearance in the core regions of the villi. Therefore, the dense appearance of dark purple areas in non-border regions of a contour indicates that this is likely a border subdividing two villi in close proximity within the contour. The light purple area identifies the cytoplasmic compartment of the SCs and CCs, along with mesenchymal support cells.

The purple class is further classified into dark purple and light purple classes. For simplicity, we call the dark purple class the "SC class". Equation (4) is used to extract the SC class, where T is the transformed matrix, and "TH" is a threshold, whose value is determined using Otsu's method [28]. The transformation of the purple class can be seen in Fig. 3. The remaining pixels are assigned to the light purple class.

$$\begin{cases} T \triangleq I_B - mean(I_G + I_R) \\ BW_{SC} = (T \geq TH) \end{cases} \quad (4)$$

2.5. Boundary detection

After extraction of the color content, the input image was separated into the background (*i.e.*, white class) and foreground (*i.e.*, all classes excluding the white class). The foreground can be adopted as a rough estimate of the boundary of the objects in the image. The binary mask from the foreground was used as initial contours in the level set algorithm, based on the Chan-Vase formulation [29], to obtain the exact boundary of each contour. The algorithm accurately segments objects of interest (i.e., villi candidates).

2.6. Villi classification

To be considered "placental villi", objects of interest needed to surpass a minimum threshold size of 1000 μm [2]. This threshold size was selected based upon well-established, healthy placenta villi dimensions previously described in the literature [30,31]. This villi size threshold is the same as the one used in work by Kidron et al. [24], which is of relevance as we are comparing our method to their method. Objects of interest <1000 μm [2] might include red and white blood cells found in the intervillous space, fibrin deposition, syncytial knots (pieces of apoptotic placenta shed from the villi surface), or artifacts from tissue processing and histological preparation.

It is important to note that there are undesired objects of interest >1000 μm [2], as demonstrated in Fig. 4a. Therefore, further descriptors

needed to be included in order to identify true placenta villi objects versus undesired objects. Mature placenta villi contain white and/or red regions within their core, indicative of the presence of connective tissue and fetal vasculature and/or fetal red blood cells (VC class). Moreover, placental villi are surrounded by a continuous layer of SC cells and a sparse underlying layer of CC cells, all of which contain dark purple nuclei (*i.e.*, SC class). Conversely, undesired objects do not have these anatomical features and therefore demonstrate a considerably different density profile for the SC and VC classes. The SC and VC class density thresholds were tuned over the training set, using density profiles of the SC and VC class of true placenta villi objects (ground truth) – as identified through manual segmentation.

2.7. Detection of touching villi

In this work, a novel approach was used to detect pairs of touching villi. The postulated boundary separating the two touching villi was identified using the presence of concavity at the site where the two villi meet, which is visually distinguishable from other concavities in a standard villous structure. Specifically, at these concave sites, you additionally see the dense presence of dark purple nuclei within the SC class. Fig. 5a shows a representative example of four placenta villi that are touching each other, with three red arrows highlighting the visual features of the concave sites of separation. In this work, villi separation boundaries were identified in two steps: 1) detection of candidate concavities through contour analysis, and 2) acceptance or rejection of each candidate concavity as a separate villous boundary, through color analysis (*i.e.*, density of different color classes in the boundary area, and the density of color classes in the two resultant villi).

1) Detection of candidate concavities

The concavity detection step employs the top-hat transform, which is defined as the subtraction of the original contour from its opening with a structuring element (SE) [32]. This definition of top-hat transform can be interpreted as an attempt to cover the areas within the contour by fitting a SE into the contour, under the condition that the entirety of the SE remains within the boundary of the contour. The areas that cannot be covered by the fitted SE are the concavities/convexities in the contour. An example is shown in Fig. 5c, where the regions that are marked in red show convexities/concavities in the contour. The output of the top-hat transform (Fig. 5d) might contain the candidate concavity (Fig. 5e), which must satisfy two conditions: 1) the removal of the candidate concavity from the contour must divide the contour into two new contours, and 2) the size of each of these new contours must satisfy the minimum villi size threshold (i.e., 1000 μm [2]). Fig. 5e shows the target concavity, which satisfies these two conditions.

Identifying candidate concavities using the top-hat transform depends on the characteristics of the SE (*i.e.*, size, shape, and alignment). Fig. 6 shows the effect of varying the characteristics of the SE on the detection of candidate concavities. In our work, an elliptical SE with different sizes and orientations (*i.e.*, 0°, 45°, 90°, and 135°) is used to detect concavities in the contour.

The procedure of changing the characteristics of the SE is continued until a candidate concavity is identified, or the top-hat transform of the contour becomes equal to the contour itself. This might happen if the size of the structuring element becomes large enough that the opening of the contour with the SE can become zero (i.e., the contour is completely eroded by the structuring element). As a result, the top-hat transform of the contour (*i.e.*, subtraction of the contour from its opening with a SE) becomes equal to its opening. If a candidate concavity is identified, the candidate concavity is removed to produce two new contours, and the concavity detection process is iteratively applied on these contours. Algorithm 1 shows the pseudocode for concavity detection.

2) Color analysis

Not all of the identified candidate concavities are actual separation boundaries between two villi. Only candidate concavities that possess certain color features are accepted as the separation boundaries. Based these color features, the border regions of a villous structure have: 1) a high density of SC cells and CC cells (*i.e.*, SC class), and 2) sparse appearance of the VC class. Therefore, candidate concavities that have high SC-class density and low density of VC-class are labeled as sepa-

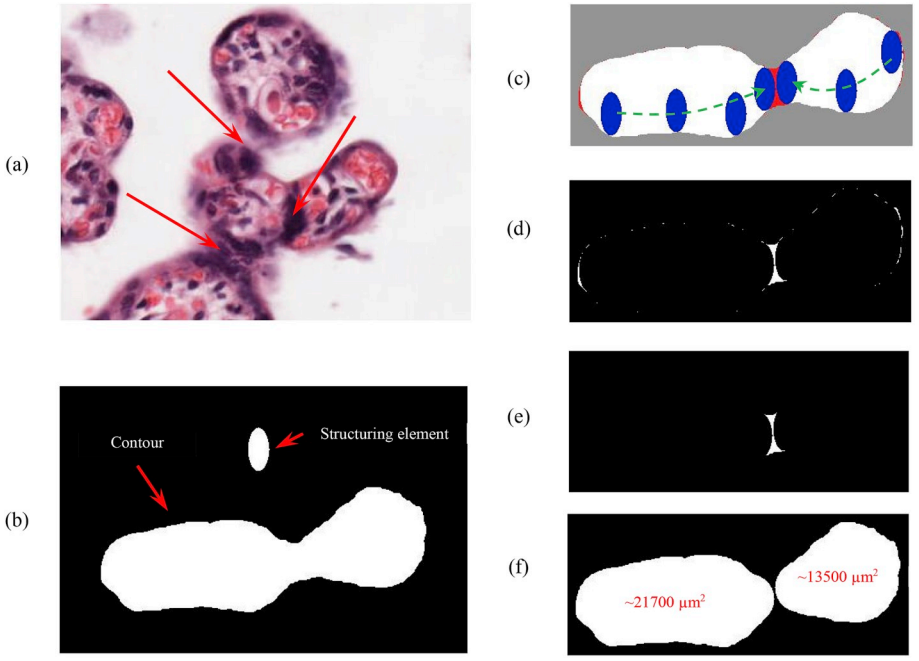

Fig. 5. (a) Examples of attachment areas in villi. (b) A sample contour and an elliptical-shape structuring element to be used in calculation of top-hat transform. (c) The interpretation of the top-hat transform by fitting the SE inside the contour. The areas that cannot be covered by SE are shown in red. These areas are the output of top-hat transform (d) The output of the top-hat transform, which represents all of the convexities and concavities in the contour. (e) The candidate concavity, which is the only concavity in the contour that its removal divide the original contour into two separate contours. (f) The resultant contours of removing the candidate concavity from the original contour. Both contour satisfied the minimum size threshold of a villous.

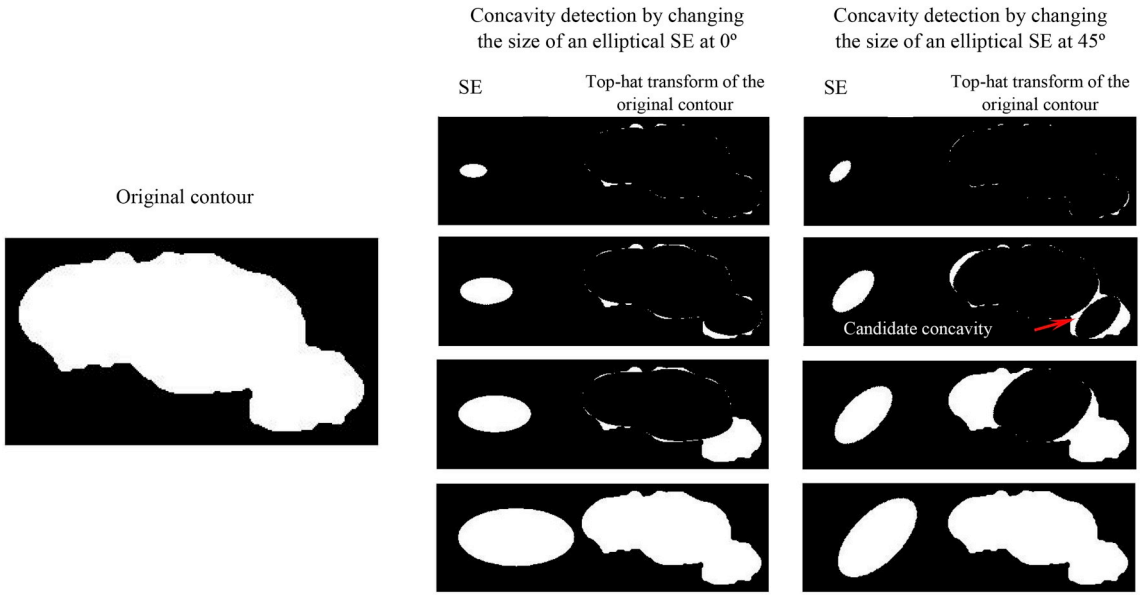

Fig. 6. An example of detecting the candidate concavity by changing the characteristics of the SE. In this example, two rotation is considered for a given elliptical-shape structuring element (*i.e.*, 0°, 45°). The size of the SE is changed for each rotation to the point that the top-hat transform of the input contour becomes equal to the input contour itself. As it can be seen in this figure, the candidate concavity cannot be detected in 0° rotation. On the other hand, in 45° rotation increasing the size of the SE leads to appearance of the candidate concavity in the top-hat transform of the contour.

Algorithm 1: Concavity detection

***Input*:** Binary mask (BW), elliptical structuring element (SE)

Output: A binary mask with all candidate concavities removed

Initialization:

Label the contours in BW → $L = \{L_0, L_1, \ldots, L_N\}$, N = number of contours

for each contour in L

  $SE = 1$

  loop of SE characteristics

    for each alignment of $SE = \{0^o, 45^o, 90^o, and\ 135^o\}$

      Calculate the Top-hat transform for contour L_i using $SE \rightarrow T_i$

      if $T_i = L_i$

        Exit nested loop of SE characteristics and go to next contour → L_{i+1}

      end if

      if the candidate concavity found in T_i

        Remove the candidate concavity from L_i to produce two new contours

        Replace L_i with one of the new contours

        Add the other new contour L_{N+1} to $L \rightarrow L = \{L_0, L_1, \ldots, L_N, L_{N+1}\}$

        Increment the number of contours $N = N + 1$

        Exit nested loop of SE characteristics and start analyzing the new contour L_i

      end if

    end for

    $SE = SE + 1$

  end loop

end for

ration boundaries. The thresholds for SC-class density and VC-class density were tuned over the training set of images, using the manual segmentation as ground truth.

2.8. Evaluation

Our data set consisted of nine images obtained from healthy term pregnancies and 27 placenta images from term pregnancies complicated with PE. We performed stratified 5-fold cross-validation, assigning the images into training and test sets with a 2:1 ratio (*i.e.*, six images from healthy patients and 18 images from PE patients were assigned to the training set, and three images from healthy patients and nine images from PE patients were assigned to the test set).

Villi detection accuracy was determined using manual segmentation as ground truth. The F1 score and sensitivity were calculated based on the following definitions:

$$Sensitivity = TP/(TP + FN) \tag{5}$$

$$F1\ score = (2 \times TP)/(2 \times TP + FP + FN) \tag{6}$$

- True positive (TP): number of villous structures identified correctly
- True negative (TN): number of objects in the binary mask generated in the boundary detection step that are correctly labeled as other objects (*i.e.*, non-villi)
- False positive (FP): number of villous structures identified incorrectly
- False negative (FN): number of villi structures identified in the manual segmentation that were not detected

For instance, if a contour contained two villi based on manual segmentation, and our algorithm correctly detected these two villi, the algorithm scored two TPs. However, if the algorithm detected only one or none of the villi, the algorithm scored one TP and one FN, or two FNs, respectively. When a contour contained only one villus based on manual segmentation, but our algorithm detected two villi, the case was scored as one TP and one FP.

2.9. Comparison to a previous method

The results of our method were evaluated against a recently published method [24] for placenta villi segmentation, based on the ImageJ software platform. The authors of the previous method publicly provided their source code online. In this previously published method, the authors extracted boundaries of villi to determine the number of existing villi in a given image, and standard color thresholding was used to segment the villi; we optimized this threshold over our training set. To achieve a fair comparison, we used the same values for the common thresholds in both methods (*i.e.*, villi size threshold, which is set to 1000 μm [2]). We then evaluated their method by comparing algorithm-generated results with manual segmentation. We also evaluate our method's segmentation results against manual segmentation and compare it with generated results from the previous method.

As stated in section II.C, TNs are defined as the number of objects in the binary mask that correctly labeled as non-villous objects. TNs were not computed for this comparison method, as it does not have a similar binary mask that would allow for a sensible TN comparison.

3. Results

As is typically observed in clinically relevant image datasets, our experimental image dataset contained artifacts and undesired objects, including imaging artifacts and maternal red blood cells in the intervillous space (12 out of 36 images were contaminated by imaging artifacts (Fig. 4)). In the villi classification step, the contours were classified based on their size and density of VC class and SC class. The proposed pipeline was able to recognize desired contours with 92.86% accuracy

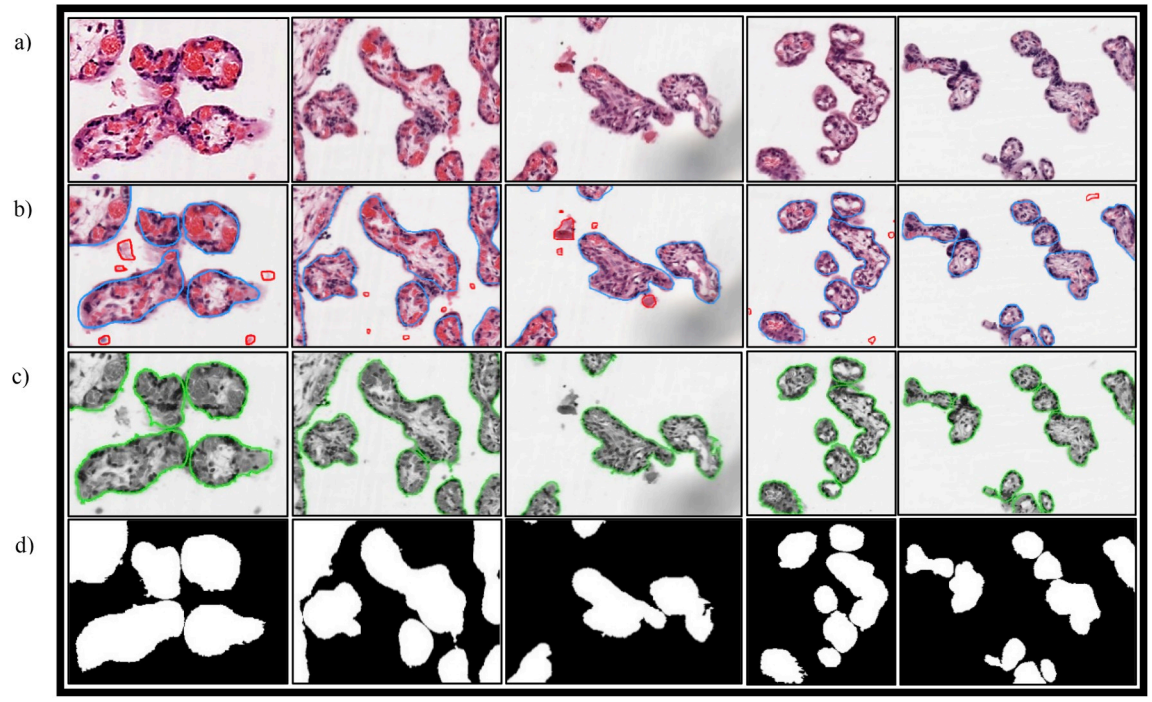

Fig. 7. Sample segmentation of villi, a) The original image, b) The manual segmentation. The boundary of a villous structure is annotated in blue. The red annotation shows undesired objects, c) The segmentation results of our proposed method. The boundaries of villi is annotated in green. d) The generated binary mask showing the final segmentation results.

Table 1
A comparison between our proposed method and the previous work. The results are presented for each fold for health term pregnancies and pregnancies complicated with PE. The TN row for the previously published work is not applicable as explained in section II.D.

		Healthy					Diagnosed with PE				
		fold #1	fold #2	fold #3	fold #4	fold #5	fold #1	fold #2	fold #3	fold #4	fold #5
Proposed method	***TP***	227	255	246	228	247	421	532	518	541	572
	TN	96	176	102	150	134	227	177	193	261	247
	FP	50	69	68	46	57	128	141	131	132	161
	FN	42	28	68	29	23	138	124	144	133	92
	F1 score (%)	83.15	84.02	78.34	85.88	86.06	75.99	80.06	79.02	80.33	81.89
	Sensitivity (%)	84.39	90.11	78.34	88.72	91.48	75.31	81.10	78.25	80.27	86.14
Previously published method [24]	***TP***	133	209	163	170	189	253	370	312	331	410
	TN	–	–	–	–	–	–	–	–	–	–
	FP	23	43	38	27	50	76	85	70	92	128
	FN	136	74	151	87	81	306	286	350	343	254
	F1 score (%)	62.59	78.13	63.30	74.89	74.26	56.98	66.61	59.77	60.35	68.22
	Sensitivity (%)	49.44	73.85	51.91	66.15	70.00	45.26	56.40	47.13	49.11	61.75

Table 2
Overall F1 score and sensitivity of the previous method, the proposed method without detection of touching villi algorithm, and the proposed method with touching villi detection algorithm. The results are reported as the weighted average of five fold cross validation.

	F1 score	*Sensitivity*
Previously published method [24]	65.30%	55.12%
Proposed method without detection of touching villi	74.58%	61.28%
Proposed method with detection of touching villi	80.76%	82.18%

(3625 out of 3904 contours were correctly identified).

Concavity detection was an important step in the detection of touching villi step. In comparison to manually identified concavities by experts, our algorithm detected concavities with an accuracy of 95.47% (3908 out of 4093 concavities were correctly identified).

Fig. 7 shows multiple sample segmentation of villi, which is performed by our proposed method. Table 1 shows the F1 scores, sensitivity, and truth table components of a recently published method [24] and the proposed method, separating the results for healthy control patients and patients diagnosed with PE. In Table 2, the overall results across all placental images are presented. In comparison to the previous method, our method yielded an F1 score and a sensitivity that are 15.46% and 27.06% higher, respectively. In order to highlight the impact that detection of touching villi has on the overall performance of our proposed method, the overall result of the proposed method without detection of touching villi is also included in Table 2.

As it is defined in Eq. (5), the sensitivity of a method depends on the total number of FNs. In this work, the majority of FN cases are generated when multiple villi are located in close proximity of each other, and the algorithm is not able to discern these as separate villi. As can be observed from the sensitivity column in Table 2, the difference gap between the previous work's sensitivity and the proposed method without detection of touching villi step is 6.68%. The comparison between the sensitivity of the proposed method with and without detection of touching villi shows a considerably large difference of 20.9%. The great improvement in sensitivity over the previous method is primarily achieved by applying the detection of touching villi step in our proposed algorithm.

The processing time required for a complete analysis of each image was approximately 21 min per image on a Core i7-6700 CPU at 3.4 GHz. We observed that this processing time is quite reasonable as the developed algorithm can run in the background without the need for any user interactions. Although we have used parallel processing in the feature-based analysis stage, the rest of the programming code is not optimized. The villi density in each image and the convexity of the extracted contours were two of the most influential factors in the determination of the processing time required for each analysis. Most of the processing time (approximately 80%) was required for the boundary detection step, which can be substantially improved by parallel (GPU) processing.

4. Discussion

An initial step for automated analysis of placental images is segmenting the chorionic villi – the functional unit of the placenta – within the histological specimens. Villi segmentation allows extraction of key features (e.g., villi count, size distribution, shape feature) for an objective assessment of placental images. Due to the complexity of villous structures and the presence of imaging artifacts, segmentation of individual villi in a placental image is a difficult task. However, the proposed method successfully identifies complex villous structures in a large series of images with high accuracy. Our proposed method yielded an F1 score of 80.76% and sensitivity of 82.18% for a dataset comprising of 4946 sample villi, which considerably outperformed a previously published method [24].

Two major contributing factors in obtaining better results in our method compared to the previous method were: 1) comprehensive artifact removal; and 2) the ability to detect and properly segment touching villi. The second factor had a large influence on the results, particularly the sensitivity score. A commonly recognized feature of the placental disease in PE is "villous agglutination" – a condition in which neighboring villi structures adhere to one another [33]. This feature of placental images from pregnancies complicated with PE likely contributed to the decreased performance of the previously published segmentation method when compared to healthy controls. Importantly, our algorithm yielded high and comparable performance when applied to histopathology cases from healthy controls (weighted average F1 score of 83.37%) or pathological cases of preeclampsia (weighted average F1 score of 79.61%) – providing confidence for the utility of this automated process in a clinical setting.

The most important limitation of our work was including connective tissue tears in VC. In our work, the calculation of fetal red blood cells density played a key role in multiple steps of our algorithm. The placental specimens used had been washed, so a considerable amount of red regions (fetal blood cells) inside placental vasculature (within the core of the villi structure) had been removed and replaced by white/light pink regions. Therefore, we also included these white regions in the calculation of VC density. However, some included areas were related to connective tissue tears, which represent no particular tissue.

The long-term goal of our work is to develop an algorithm that has the ability to process the whole placenta scan. This can be achieved by block analysis. With the scans used in our dataset, on average, around 50 extracted images would be required to cover the whole scan. Although the presented pipeline has the potential to analyze the entire scans (i.e., analysis of ~50 images per scan), in our study, we only present the results from three images from each placental scan. Manual segmentation,

to establish a ground truth, is a time-consuming process, and it was believed that it was more important for this study to have images that better capture the variability across scans than within a scan.

5. Conclusion

In this study, a fully automated method for segmentation of chorionic villi structures in histopathology images of the human placenta was presented. The proposed method has the ability to identify complex villous structures, including touching and overlapping villi, by performing color analysis on the detected concavities of the villi structures. Our proposed method yielded an F1 score of 80.76% and sensitivity of 82.18% for a dataset comprising of nearly 5000 sample villi, considerably higher performance than previously published methods. In addition, the proposed method has a comparable performance on placental samples from healthy and pathological pregnancies, a critical consideration in determining clinical utility.

With the help of an accurate and robust automated analysis method, pathologists might be presented with a set of otherwise inaccessible morphometric values for each image, such as the distribution of specific structures (physically and class-wise) and presence or absence of certain histological features/findings within identified structures. The pathologist can use these values to help make a final diagnosis. Although we focused only on histopathology images of the placenta, it might be possible to generalize this tool across multiple fields of clinical pathology. This could result in a marketable tool that would substantially reduce the subjectivity that exists in current practice.

Conflicts of interest

None.

Acknowledgments

This work is supported in part by the Ontario Trillium Scholarship (OTS) and Natural Sciences and Engineering Research Council (NSERC) of Canada.

References

[1] B. Huppertz, Placental pathology in pregnancy complications, Thromb. Res. (2011), https://doi.org/10.1016/S0049-3848(11)70026-3.
[2] R.I. Sava, K.L. March, C.J. Pepine, Hypertension in pregnancy: taking cues from pathophysiology for clinical practice, Clin. Cardiol. (2018), https://doi.org/10.1002/clc.22892.
[3] M. Kovo, L. Schreiber, A. Ben-Haroush, E. Gold, A. Golan, J. Bar, The placental component in early-onset and late-onset preeclampsia in relation to fetal growth restriction, Prenat. Diagn. (2012), https://doi.org/10.1002/pd.3872.
[4] J.M. Roberts, C. Escudero, The placenta in preeclampsia, Pregnancy Hypertens (2012), https://doi.org/10.1016/j.preghy.2012.01.001.
[5] T.K. Morgan, Role of the placenta in preterm birth: a review, Am. J. Perinatol. (2016), https://doi.org/10.1055/s-0035-1570379.
[6] R. Bukowski, M. Carpenter, D. Conway, et al., Causes of death among stillbirths, JAMA, J. Am. Med. Assoc. (2011), https://doi.org/10.1001/jama.2011.1823.
[7] L. Bellamy, J.-P. Casas, A.D. Hingorani, D.J. Williams, Pre-eclampsia and risk of cardiovascular disease and cancer in later life: systematic review and meta-analysis, BMJ (2007), https://doi.org/10.1136/bmj.39335.385301. BE.
[8] H a de Boo, J.E. Harding, The developmental origins of adult disease (Barker) hypothesis, Aust. N. Z. J. Obstet. Gynaecol. (2006), https://doi.org/10.1111/j.1479-828X.2006.00506.x.
[9] R.W. Redline, Classification of placental lesions, Am. J. Obstet. Gynecol. 213 (4) (2015) S21–S28, https://doi.org/10.1016/j.ajog.2015.05.056.
[10] A. Chen, D.J. Roberts, Placental Pathologic Lesions with a Significant Recurrence Risk - what Not to Miss! *APMIS*, 2017.
[11] J.M. Catov, C.M. Scifres, S.N. Caritis, M. Bertolet, J. Larkin, W.T. Parks, Neonatal outcomes following preterm birth classified according to placental features, Am. J. Obstet. Gynecol. (2017), https://doi.org/10.1016/j.ajog.2016.12.022.
[12] M.T. Vinnars, J. Nasiell, G. Holmström, M. Norman, M. Westgren, N. Papadogiannakis, Association between placental pathology and neonatal outcome in preeclampsia: a large cohort study, Hypertens. Pregnancy (2014), https://doi.org/10.3109/10641955.2013.842584.
[13] A.M. Roescher, A. Timmer, J.J.H.M. Erwich, A.F. Bos, Placental pathology, perinatal death, neonatal outcome, and neurological development: a systematic review, PLoS One (2014), https://doi.org/10.1371/journal.pone.0089419.
[14] K.M. Chisholm, A. Heerema-Mckenney, Fetal thrombotic vasculopathy: significance in liveborn children using proposed society for pediatric pathology diagnostic criteria, Am. J. Surg. Pathol. (2015), https://doi.org/10.1097/PAS.0000000000000334.
[15] R.W. Redline, The clinical implications of placental diagnoses, Semin. Perinatol. 39 (1) (2015) 2–8, https://doi.org/10.1053/j.semperi.2014.10.002.
[16] P. Kelehan, A. Maes, E.M. Mckay, T.K. Morgan, P.G.J. Nikkels, Sampling and Definitions of Placental Lesions, vol. 140, 2016, https://doi.org/10.5858/arpa.2015-0225-CC. July.
[17] R.W. Redline, Placental Pathology: A Systematic Approach with Clinical Correlations, vol. 22, 2008, pp. 86–91, https://doi.org/10.1016/j.placenta.2007.09.003.
[18] R.W. Redline, Villitis of unknown etiology: noninfectious chronic villitis in the placenta, Hum. Pathol. (2007), https://doi.org/10.1016/j.humpath.2007.05.025.
[19] G. Turowski, L.N. Berge, L.B. Helgadottir, E.M. Jacobsen, B. Roald, A new, clinically oriented, unifying and simple placental classification system, Placenta (2012), https://doi.org/10.1016/j.placenta.2012.10.002.
[20] B. Hargitai, Best practice NO 178: examination of the human placenta, J. Clin. Pathol. (2004), https://doi.org/10.1136/jcp.2003.014217.
[21] S.L. Warsof, P. Gohari, R.L. Berkowitz, J.C. Hobbins, The estimation of fetal weight by computer-assisted analysis, Am. J. Obstet. Gynecol. (1977), https://doi.org/10.1016/0002-9378(77)90058-8.
[22] N. Almoussa, B. Dutra, B. Lampe, et al., Automated vasculature extraction from placenta images, Proc. SPIE-Int. Soc. Opt. Eng. 7962 (2011), https://doi.org/10.1117/12.878343, 79621L-79621L - 10.
[23] Z. Swiderska-Chadaj, T. Markiewicz, R. Koktysz, S. Cierniak, Image processing methods for the structural detection and gradation of placental villi, Comput. Biol. Med. (April) (2017) 1–11, https://doi.org/10.1016/j.compbiomed.2017.08.004.
[24] D. Kidron, I. Vainer, Y. Fisher, R. Sharony, Automated image analysis of placental villi and syncytial knots in histological sections, Placenta 53 (2017) 113–118, https://doi.org/10.1016/j.placenta.2017.04.004.
[25] J.M. Chang, N. Huynh, M. Vazquez, C. Salafia, Vessel enhancement with multiscale and curvilinear filter matching for placenta images. International Conference on Systems, Signals, and Image Processing, 2013, pp. 125–128, https://doi.org/10.1109/IWSSIP.2013.6623469.
[26] P. Palee, B. Sharp, L. Noriega, N.J. Sebire, C. Platt, Image analysis of histological features in molar pregnancies, Expert Syst. Appl. 40 (17) (2013) 7151–7158, https://doi.org/10.1016/j.eswa.2013.06.034.
[27] G.D. Finlayson, B. Schiele, J.L. Crowley, Comprehensive colour image normalization, in: Lecture Notes in Computer Science (Including Subseries Lecture Notes in Artificial Intelligence and Lecture Notes in Bioinformatics), 1998, https://doi.org/10.1007/BFb0055685.
[28] O. Nobuyuki, A threshold selection method from gray-level histograms, IEEE Trans. Syst. Man Cybern. (1979), https://doi.org/10.1109/TSMC.1979.4310076.
[29] T.F. Chan, L.A. Vese, Active contours without edges, IEEE Trans. Image Process. 10 (2) (2001) 266–277, https://doi.org/10.1109/83.902291.
[30] F. Stoz, R.A. Schuhmann, A. Schmid, Morphometric investigations of terminal villi of diabetic placentas in relation to the White classification of diabetes mellitus, J. Perinat. Med. 440 (1987) 193–198.
[31] S. Chaikitgosiyakul, M.J. Rijken, A. Muehlenbachs, et al., A morphometric and histological study of placental malaria shows significant changes to villous architecture in both *Plasmodium falciparum* and *Plasmodium vivax* infection, Malar. J. (2014) 1–13.
[32] R.M. Haralick, S.R. Sternberg, X. Zhuang, Image analysis using mathematical morphology, IEEE Trans. Pattern Anal. Mach. Intell. (1987), https://doi.org/10.1109/TPAMI.1987.4767941.
[33] M.W. Stark, L. Clark, R.D. Craver, Histologic differences in placentas of preeclamptic/eclamptic gestations by birthweight, placental weight, and time of onset, Pediatr. Dev. Pathol. 17 (3) (2014) 181–189, https://doi.org/10.2350/13-09-1378-OA.1.